Voltage-Activated Calcium Signals in Myotubes Loaded with High Concentrations of EGTA

R. P. Schuhmeier, B. Dietze, D. Ursu, F. Lehmann-Horn, and W. Melzer
Universität Ulm, Abteilung für Angewandte Physiologie, D-89069 Ulm, Germany

ABSTRACT In the present study we describe the analysis of optically recorded whole cell Ca^{2+} transients elicited by depolarization in cultured skeletal myotubes. Myotubes were obtained from the mouse muscle-derived cell line C2C12 and from mouse satellite cells. The cells were voltage-clamped and perfused with an artificial intracellular solution containing 15 mM EGTA to ensure that the bulk of the Ca^{2+} mobilized by depolarization is bound to this extrinsic buffer. The apparent on- and off-rate constants of EGTA and the dissociation rate constant of fura-2 in the cell were estimated by investigating the Ca^{2+}-dependence of kinetic components of the fluorescence decay after repolarization. These parameters were used to calculate the time course of the total voltage-controlled flux of Ca^{2+} to the myoplasmic space (Ca^{2+} input flux). The validity of the procedure was confirmed by model simulations using artificial Ca^{2+} input fluxes. Both C2C12 and primary-cultured myotubes showed a very similar phasic-tonic time course of the Ca^{2+} input flux. In most measurements, the input flux was considerably larger and showed a different time course than the estimated Ca^{2+} flux carried by the L-type Ca^{2+} channels, indicating that it consists mainly of voltage-controlled Ca^{2+} release from the sarcoplasmic reticulum. In cells with extremely small fluorescence transients, the calculated input fluxes matched the kinetic characteristics of the Ca^{2+} inward current, indicating that Ca^{2+} release was absent. These measurements served as a control for the fidelity of the fluorimetric flux analysis. The procedures promise a deeper insight into alterations of Ca^{2+} release gating in studies employing myotube expression systems for mutant or chimeric protein components of excitation-contraction coupling.

INTRODUCTION

Voltage-controlled Ca^{2+} fluxes are primary events during the activation of muscle cells (Melzer et al., 1995; Bers, 2001). A rapid depolarization-activated Ca^{2+} inward current triggers Ca^{2+} release in cardiac cells (Wang et al., 2001), whereas in skeletal muscle, Ca^{2+} release is activated first, followed by a Ca^{2+} current of much slower kinetics (Brum et al., 1987; Friedrich et al., 1999; Szentesi et al., 2001). In skeletal muscle cells, a direct protein-protein interaction between the α_1 subunit (α_{1S}) of the transverse tubular dihydropyridine receptor and the ryanodine receptor (RyR1) appears to be responsible for the activation of Ca^{2+} release and for a retrograde enhancement of the Ca^{2+} current (Grabner et al., 1999; Dirksen, 2002).

To identify structural determinants of excitation-contraction (EC) coupling, oligo-nucleated skeletal myocytes in culture (myotubes) have been extensively used for functional expression of chimeric and mutant proteins (e.g., García et al., 1994; Beam and Franzini-Armstrong, 1997). In particular, myotubes of the dysgenic and the dyspedic mouse, which are deficient in α_{1S} and RyR1, respectively (Chaudhari, 1992; Takekura et al., 1995), have been employed. Corresponding permanent cell lines, GLT (Powell et al., 1996) and 1B5 (Moore et al., 1998) have also been generated and applied (e.g., Jurkat-Rott et al., 1998; Flucher et al., 2000; Fessenden et al., 2000).

The analysis of voltage-controlled Ca^{2+} release in myotubes lags behind studies of mature muscle fibers that provided most of the available information on this process (for reviews see e.g., Schneider, 1994; Baylor and Hollingworth, 2000; Ríos and Brum, 2002). Clearly, the kinetics of the release process in myotubes has to be studied in detail to fully evaluate alterations in EC coupling caused by the expression of mutant proteins. In the present investigation we carried out whole-cell patch-clamp experiments to control the membrane potential of myotubes that contained a millimolar concentration of EGTA as the major intracellular Ca^{2+} buffer, and we analyzed the kinetics of fura-2 fluorescence transients induced by step depolarization. Most of our experiments were conducted on myotubes derived from the C2C12 cell line. This diploid continuous cell line was established by subcloning the C2 cell line (Blau et al., 1983) originally derived from primary-cultured leg muscles of a C3H mouse (Yaffe and Saxel, 1977). It has become a frequently used model system to study skeletal muscle-specific events in differentiation and function.

The high concentration of intracellular EGTA used in our experiments ensures that most of the mobilized Ca^{2+} is bound to EGTA. Quantification of the time course of the Ca^{2+} mobilization (Ca^{2+} input flux), therefore, depends on the knowledge of the dynamic behavior of EGTA in the cell. Song et al. (1998) conducted a kinetic analysis on EGTA-loaded heart cells that allowed them to experimentally derive the apparent dissociation rate constant of EGTA ($k_{off,EGTA}$) in the cell. Here we applied a modified version of this method that permits to estimate both $k_{on,EGTA}$ and $k_{off,EGTA}$. In

Submitted August 26, 2002, and accepted for publication October 16, 2002.

Address reprint requests to Werner Melzer, Univ. of Ulm, Dept. of Applied Physiology, Albert-Einstein-Allee 11, D-89069 Ulm, Germany. Tel: ++49-731-500-23248; Fax: ++49-731-500-23260; E-mail: werner.melzer@medizin.uni-ulm.de.

0006-3495/03/02/1065/14 $2.00

addition we determined the kinetic behavior of fura-2 for our experimental conditions. These kinetic parameters were used to derive the time course of total Ca^{2+} input flux to the myoplasm during pulse depolarization.

METHODS

Cell culture

C2C12 cells were purchased from the American Tissue Culture Collection (CRL-1772). Myoblasts were grown in Dulbecco's modified Eagle's medium with high glucose and 10% fetal calf serum (FCS) in 25 mm^2 culture flasks. At two- to three-day intervals (i.e., when ~80% confluency was reached) cells were detached by trypsin treatment (0.25%) in Ca^{2+}- and Mg^{2+}-free phosphate-buffered saline and reseeded after dilution (1:5 or 1:10) in fresh growth medium.

To obtain myotubes, collagen-coated flasks were used and FCS in the medium was replaced by 2% horse serum 8–24 h after seeding. After one to two weeks in the differentiation medium, myotubes were detached by trypsin and seeded onto coverslips (22 × 22 mm, 0.17 mm thickness; Menzel-Gläser, Braunschweig, Germany) in 35-mm petri dishes. The coverslips were carbon-coated and subsequently ionized in a vacuum evaporation system (Model 306, BOC Edwards, Crawley, UK). To stabilize the carbon layer and for sterilization, the coverslips were heated at 185°C for 8 h. The carbon-coated sterile coverslips were covered with collagen to further improve cell adhesion.

The trypsin detachment followed by reattachment resulted in myotubes that were more compact than before the treatment and therefore better suited for patch clamping. Measurements were carried out one to two days after myotubes had been reseeded. Primary cultures of mouse myotubes were carried out as described by Ursu et al. (2001).

Dulbecco's modified Eagle's medium and trypsin were purchased from Gibco (Karlsruhe, Germany); FCS, horse serum, and phosphate-buffered saline from PAA Laboratories (Cölbe, Germany); and rat tail collagen (Typ 1, C 7661) from Sigma (Deisenhofen, Germany).

Experimental solutions

The solutions for patch-clamp measurements had the following composition (in mM): Bathing solution—140 tetraethylamonium hydroxide, 137 HCl, 10 $CaCl_2$, 1 $MgCl_2$, 10 HEPES, 2.5 4-aminopyridine, 0.00125 tetrodotoxin, pH adjusted to 7.4 with HCl. Pipette solution—145 CsOH, 110 HCl, 1.5 $CaCl_2$, 10 HEPES, 15 EGTA, 4 MgATP (5.5 total Mg), 5 Na creatine phosphate, 0.2 K_5-fura-2, pH adjusted to 7.2 with CsOH. 1 ml aliquots of the pipette solution (without fura-2) were stored frozen at −20°C. Solutions were filtered before use (pore size 0.25 μm).

Electrophysiology and data acquisition

Size (membrane capacitance ~300 pF), compact shape, and a smooth surface were selection criteria to choose cells for the experiments. Myotubes were voltage-clamped in the whole-cell configuration with a patch-clamp amplifier (LMPC, List-Medical, Darmstadt-Eberstadt, Germany) with extended range of capacitance compensation (1000 pF). Pipettes were pulled from borosilicate glass (GC150TF-10, Clark Electromedical Instruments, Reading, UK) and the tips were fire polished. The pipettes had resistances between 1.5 and 2 MΩ when filled with the artificial intracellular solution. Simultaneously measured fluorescence and membrane current records were sampled at 4 kHz using a DA-AD interface (Digidata 1200, Axon Instruments, Union City, CA, USA) connected to a Pentium computer. The experiments were carried out at room temperature (20–23°C). For data acquisition, the pCLAMP 7.0 software package (Axon Instruments) was used.

Fluorimetry

Optical measurements were carried out using a photomultiplier tube (R268, Hamamatsu) attached to the trinocular head of an inverted microscope (Axiovert 100 with Objective ''Fluar'' 40 × 1.30 Oil, Zeiss, Germany). The cells were loaded with the indicator dye fura-2 by diffusion from the patch pipette. Fluorescence was excited at 380 nm (for Ca^{2+} signals) and 360 nm (isosbestic point) using interference filters of bandwidth 14 and 10 nm, respectively (Schott Glaswerke, Mainz, Germany, and Andover Corp., Salem, NH, USA) and was measured at 515 nm (bandwidth 30 nm, Zeiss, Oberkochen, Germany). Changes in free Ca^{2+} concentration were determined using the background-corrected ratio R (see Results) of the fluorescence signals ($R = F_{380}/F_{360}$) at the two excitation wavelengths and taking into account fura-2 kinetics according to Eq. 1:

$$[Ca^{2+}] = K_{D,Fura} \cdot \left[\frac{\frac{1}{k_{off,Fura}} \cdot \frac{dR}{dt} + R - R_{min}}{R_{max} - R} \right]. \quad (1)$$

Here R_{min} and R_{max} are the limiting ratio levels corresponding to Ca^{2+}-free and fully Ca^{2+}-saturated dye. $K_{D,Fura}$ is the Ca^{2+} dissociation constant of fura-2 and $k_{off,Fura}$ the dissociation rate constant. For equilibrium in vitro calibrations, we used internal solutions with different free Ca^{2+} concentrations (buffered by 15 mM EGTA and containing 0.2 mM fura-2). The measurements were carried out in an experimental setting very similar to the whole-cell recordings. Small droplets (different diameters up to ~200 μm) of the calibration solution were applied from a patch pipette onto carbon-coated coverslips covered with a high viscosity silicone grease (Baysilone, Bayer, Leverkusen, Germany), and fluorescence was recorded with our microscope fluorimeter from areas of 50 μm × 50 μm. At each Ca^{2+} concentration, F_{380} was proportional to F_{360} when changing the droplet size, indicating that inner filter effects were insignificant. The ratio R was obtained from the slope of the F_{380} versus F_{360} plot determined by linear regression. R, plotted as a function of free Ca^{2+} concentration, was fitted with Eq. 2 and gave the following estimates for R_{min}, R_{max}, and $K_{D,Fura}$: 2.69 ± 0.02, 0.77 ± 0.02, and 276 ± 22 nM, respectively.

$$R = \frac{\frac{[Ca^{2+}]}{K_{D,Fura}} \cdot R_{max} + R_{min}}{\frac{[Ca^{2+}]}{K_{D,Fura}} + 1}. \quad (2)$$

In vivo estimates of R_{max} and R_{min} were obtained as follows: Ratio values for full dye saturation in the cell (R_{max}) were determined by perfusing myotubes with intracellular solutions of elevated Ca^{2+} concentration (2.7 mM free) and applying additional electrical stimuli to release stored Ca^{2+}. R_{max} obtained in this way was 0.68 ± 0.03 ($n = 4$). R_{min} was calculated using estimates of the intracellular fluorescence ratio values R_0 at the beginning of the experiment (see Results). The mean value of R_0 in 62 cells was 2.69 ± 0.02. Assuming that the intracellular concentration during perfusion was identical to the buffered-free Ca^{2+} concentration in the pipette solution (20 nM) and using the $K_{D,Fura}$ value determined in vitro (276 nM), we calculated R_{min} according to Eq. 2. The result was 2.84 ± 0.02. A comparison shows that these R_{max} and R_{min} values differ only slightly from the ones determined in vitro. The in vivo values were used in the analysis of measured fluorescence signals.

Volume-capacitance ratios (V_C) were determined in voltage-clamped C2C12 myotubes that were loaded with the indicator fluo-3 and imaged with a confocal laser scanning microscope (Radiance 2000, Bio-Rad, Hemel Hempstead, UK) using the 488 nm Argon laser line.

Numerical analysis

General analysis and nonlinear curve fitting were carried out using Excel (Microsoft) and Origin (OriginLab, Northampton, MA, USA). Free

concentrations of Mg^{2+} and Ca^{2+} were calculated using the program CalcV22 (Föhr et al., 1993). Simulations and numerical calculations of the total flux of Ca^{2+} into the myoplasm (Ca^{2+} input flux) from fluorescence measurements were carried out using a program written in Delphi (Borland, Scotts Valley, CA, USA) assuming the presence of fura-2 (0.2 mM), EGTA (15 mM), and optionally troponin C with 0.24 mM of fast Ca^{2+}-specific T sites and 0.24 mM of slow Ca^{2+} Mg^{2+} sites with parvalbumin-type behavior (P sites) rate constants from Baylor and Hollingworth, 1998; differential equations, see Baylor et al., 1983, and Brum et al., 1988. For parameter values used in the calculations, see Results (Fig. 6 legend).

The calculation routines implemented digital filtering using two different algorithms to estimate the ratio *R* and its first time derivative from noisy data. A second order Savitzky-Golay filter (Savitzky and Golay, 1964; Ratzlaff, 1987) of fixed bandwidth (5 ms) was normally used. Three successive filter runs were applied on each trace leading to a better elimination of high frequencies than just one run at higher bandwidth. In addition, a second filter algorithm was designed to automatically vary the bandwidth by estimating the local signal to noise relation. The filter uses a variable bandwidth kernel estimator as described in Müller and Stadtmüller (1987). However, instead of varying a globally optimized bandwidth (Rice, 1984; Timmer et al., 1998), an optimal local bandwidth was chosen by limiting the local bias of the filtered signal. To estimate the time course of the signal, its first and its second time derivative, we used kernels that were calculated by multiplying the cosine function plus offset with a constant, a linear, and a parabolic function, respectively. Commonly used polynomial kernels (boxcar and higher order as described in Ratzlaff, 1987; Gasser et al., 1985) showed similar results. This filter performed well on very noisy records due to its ability to track fast signal components and to strongly smooth regions with slow signal alterations (see Fig. 8 *E* and Fig. 9, *F–H*).

Unless otherwise stated, data are presented and plotted as ''mean ± SE (n = number of experiments)'' for averaged values and as ''parameter ± SE'' for best-fit parameters.

RESULTS

Time course of cell loading and corrections for background light and bleaching

Fig. 1 demonstrates the time course of indicator loading by diffusion from the patch pipette in a C2C12 myotube. Resting fluorescence measurements were carried out within a time interval of 25 min. Excitation light was altered between 360 and 380 nm. Initially, the fluorescence level was high due to indicator leak from the tip of the pipette when approaching the cell. After sealing the tip to the membrane and washing away the external indicator, the fluorescence at the two excitation wavelengths settled to lower constant values resulting from cellular autofluorescence and fluorescence of the dye-loaded patch pipette. When access to the cytoplasm was obtained by breaking the patch (at time 0), fluorescence started to rise again until it reached a saturation level due to the spread of the indicator dye within the cell.

In Fig. 1 *B*, the background light level was subtracted and the fluorescence ratio F_{380}/F_{360} was calculated. The figure shows that despite the rise in indicator concentration, the ratio and therefore the resting free Ca^{2+} level remained stable over the whole observation interval. In Fig. 1 *C*, the fluorescence measurements at the two excitation wavelengths are plotted versus each other for the first 5 min of the experiment. The intersection of the two lines marks the

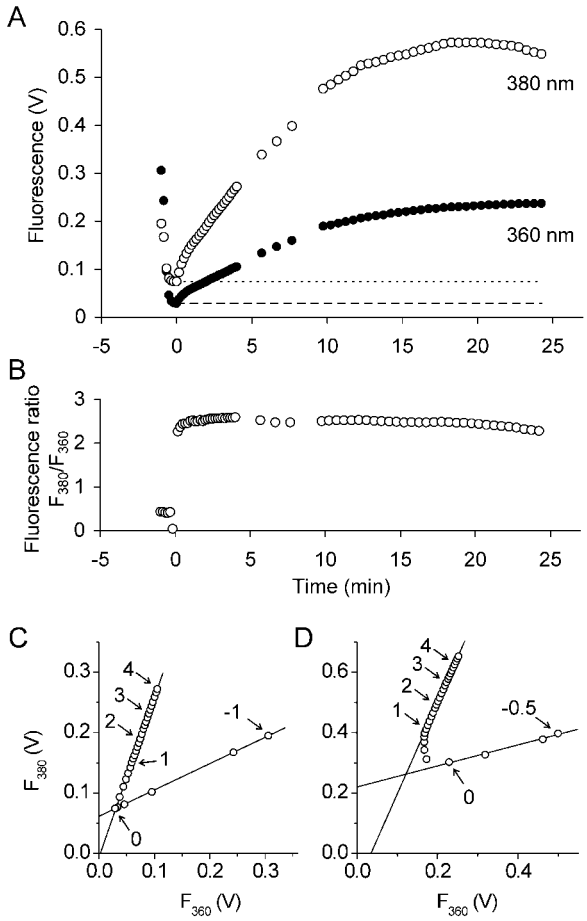

FIGURE 1 Time course of solution exchange in a voltage-clamped myotube and determination of background light intensity. (*A*) Alternating measurements of 515 nm fluorescence of fura-2 at excitation wavelengths of 360 nm (isosbestic) and 380 nm. Dotted and dashed horizontal lines indicate background light levels. (*B*) Ratio F_{380}/F_{360} after background light subtraction (see below). (*C*) F_{380} plotted versus F_{360} shows linear relations and intersection of the lines at the background intensity levels. The different slopes of the lines show that the background-corrected ratio F_{380}/F_{360} changed from a constant low value of 0.44, due to full dye saturation by the high Ca^{2+} concentration in the external solution, to a constant higher value of 2.64 after breaking the patch, resulting from the EGTA-buffered low Ca^{2+} concentration in the pipette solution. (*D*) Similar experiment as in *C* but dye entry started before the background light level could be determined. Linear extrapolation of the F_{380} versus F_{360} plots permits estimating the background light intensities. Arrows in *C* and *D* indicate time in minutes relative to the moment of establishing the whole cell configuration.

background light intensities. The F_{380} versus F_{360} plots made it possible to determine background light levels also in cases when the cell opened before the external dye could be completely washed away. The background values were then obtained from the intersection of the two extrapolated lines as shown in Fig. 1 *D*. The means of the corresponding ratio values for low and full Ca^{2+} saturation of the dye, determined from the slopes of the lines, were 2.69 ± 0.02 (= R_0, see Methods, n = 62) and 0.46 ± 0.01 (n = 54), respectively.

Fig. 2 *A* shows our experimental protocol to measure depolarization-induced Ca^{2+} signals. The cell was illuminated sequentially by the two excitation wavelengths 360 and 380 nm (*horizontal bars*, *bottom*). During the 380-nm interval, the cell was activated by a voltage clamp depolarization (*a*) that elicited Ca^{2+} inward current (*b*) and a fluorescence decrease resulting from the increase in intracellular Ca^{2+} concentration (*c*). A slow decline in fluorescence due to dye bleaching could be observed in most experiments. Even though this decline was generally small, it can influence the kinetic analysis described below. To correct for the loss of dye resulting from the irradiation, a single exponential function with time constant τ and end value 0 was fitted to the baseline preceding the voltage pulse of the background-corrected 380-nm record. For the ratio calculation during the 380-nm illumination interval, a virtual 360-nm record was calculated as a scaled-down version of the same exponential function. The scaling factor was F_{360}/F_{380} determined using the linearly extrapolated background-corrected intensities (*open and closed circle*) at the time indicated by the arrow. Fig. 2 *B* demonstrates the procedure for a measurement containing a 100-ms pulse from −90 to +20 mV (*a*). Panel *b* shows the inward current and panel *c* the 380-nm signal before (*left*) and after (*right*) correction for bleaching.

Determining EGTA kinetics in the cell

The determination of the Ca^{2+} input flux from measured Ca^{2+} transients requires the knowledge of Ca^{2+} binding to intrinsic binding sites (Baylor et al., 1983). The advantage of introducing an extrinsic buffer of high concentration is that the determination of Ca^{2+} input flux becomes largely independent of intrinsic Ca^{2+} buffering as shown by Ríos and co-workers in their work on frog skeletal muscle fibers (González and Ríos, 1993, see also Pape et al., 1995; Struk et al., 1998). It also prevents contractile activation and movement artifacts. In the present study we used 15 mM EGTA in the pipette solution. When EGTA dominates intracellular binding, free Ca^{2+} exhibits a time course that shows kinetic characteristics of the Ca^{2+} input flux (Ríos and Pizarro, 1991; Song et al., 1998). A calculation by Song et al. (1998) showed that the change in free Ca^{2+} (f) in a cell loaded with a sufficiently high EGTA concentration is approximately the sum of a term f_r proportional to the Ca^{2+} input flux and a term f_s proportional to its time integral ($f = f_r + f_s$ and $f_s = \alpha \cdot \int f_r\, dt$). This group demonstrated that the proportionality factor α of the integral term, which can be determined from the fluorescence measurements, allows the calculation of the EGTA dissociation rate constant $k_{off,EGTA}$ in the cell according to Eq. 3:

$$\alpha = k_{off,EGTA} \cdot \left(1 + \frac{[Ca^{2+}]_0}{K_{D,EGTA}}\right). \quad (3)$$

Here $[Ca^{2+}]_0$ is the baseline free Ca^{2+} concentration and $K_{D,EGTA}$ the apparent Ca^{2+} dissociation constant of EGTA.

Fig. 3 shows the procedure to derive α from our experimental records. For an approximate first determination of α, we converted the fluorescence ratio signal (Fig. 3 *B*) to linear Ca^{2+} ($Ca^{2+}{}_L$) using the steady-state version of Eq. 1 (i.e., with $dR/dt = 0$). The $Ca^{2+}{}_L$ record (Fig. 3 *C*) therefore is a low-pass-filtered version of free Ca^{2+}. However, as will be shown below (Fig. 4), using $Ca^{2+}{}_L$ instead of free Ca^{2+} makes only a small difference in the determination of α.

Similar as Song et al (1998), we consider $F = [Ca^{2+}{}_L] - [Ca^{2+}]_0$ as the sum of a function F_r and a term F_s, which is the product of α and the running time integral of F_r (i.e., $F = F_r + F_s$; $F_s = \alpha \cdot \int F_r\, dt$). α was determined by fitting a monotonously rising integral term F_s to the pedestal level at the end of the transient F. To achieve this, the integral equation $F_r = F - \alpha \cdot \int F_r\, dt$ was numerically solved for F_r with α as a free parameter. α was altered by iteration to ensure that F_r deviated minimally from zero in the interval 100–300 ms after the end of the pulse. After convergence of the fit, F_s resulted as the difference between F and the best-fit function F_r (Fig. 3 *C*).

Song et al. (1998) used α to calculate an apparent $k_{off,EGTA}$ according to Eq. 3 by assuming intracellular values for $[Ca^{2+}]_0$ and $K_{D,EGTA}$. In the present study, the use of a ratiometric dye permitted to study the $[Ca^{2+}]_0$ dependence of α and to determine both rate constants $k_{off,EGTA}$ and $k_{on,EGTA}$ by linear least squares fitting using Eq. 4, which is identical to Eq. 3.

$$\alpha = k_{off,EGTA} + k_{on,EGTA} \cdot [Ca^{2+}]_0. \quad (4)$$

Fig. 3 *D* shows the result. The best-fit parameter values were $k_{off,EGTA} = 2.73 \pm 0.30\ s^{-1}$ and $k_{on,EGTA} = 49.8 \pm 7.6\ \mu M^{-1}\ s^{-1}$, respectively.

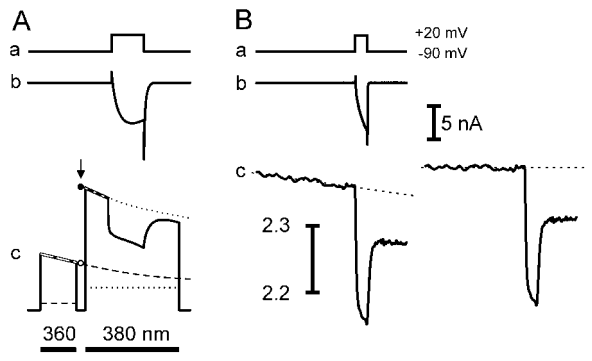

FIGURE 2 Pulse protocol and bleaching correction. (*A*) Schematic diagram showing the timing of voltage pulse application and illumination for fluorescence excitation and the procedure for bleaching correction. The bleaching time course was described by single exponential functions of identical time constant τ approaching the background levels determined at the beginning of the experiment (see text for more explanation). (*B*) Demonstration of bleaching correction. (*a*) Voltage (pulse duration 100 ms), (*b*) current record, (*c*) F_{380} record before (*left*) and after (*right*) correction for bleaching.

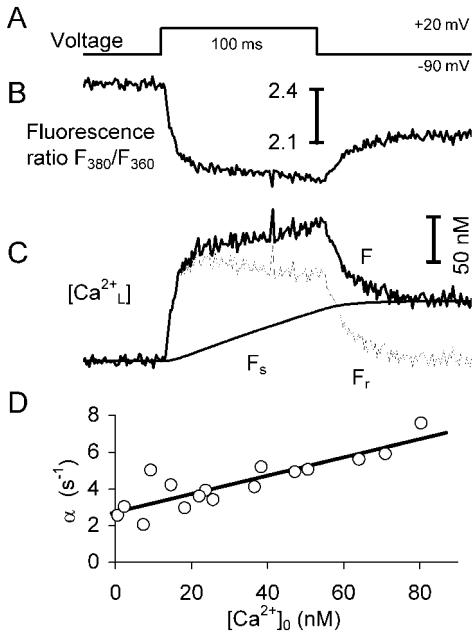

FIGURE 3 Determination of on- and off-rate constant of EGTA in the cell. (*A*) Voltage pulse from −90 to +20 mV (100 ms). (*B*) Fluorescence ratio record. (*C*) "Linear Ca^{2+}" ($[Ca^{2+}_L]$) before (*thick noisy record*: *F*) and after (*thin noisy record*: F_r) subtraction of the integral component F_s (see text for explanation). (*D*) Scaling factor α of the integral component F_s as a function of baseline free Ca^{2+}. $k_{on,EGTA}$ and $k_{off,EGTA}$ are obtained as best-fit parameters from the linear regression using Eq. 4 (*continuous line*).

To check the reliability of the method, we applied a model simulation and investigated whether the EGTA rate constants used in the simulation can be correctly determined. This is demonstrated in Fig. 4.

Artificial Ca^{2+} flux curves were constructed using a combination of rectangular pulses (Fig. 4 *A*) and were used as inputs to a system containing 200 μM fura-2 and 15 mM EGTA. In the simulations, short (10 ms) prepulses of different amplitudes generated different baseline levels of free Ca^{2+} concentration. Each prepulse was followed by the same test pulse paradigm consisting of a short initial pulse (10 ms) of relatively large amplitude (10 μM ms^{-1}) and a four-times smaller adjacent step of 90-ms duration. The phasic shape of the input flux signal was necessary to generate artificial fluorescence signals similar to the ones observed in the experiments (see Fig. 5 *A*). The off-rate constant of fura-2 was assumed to be 30 s^{-1} (close to the value of 26 s^{-1} reported by García and Schneider (1993) for rat fibers. $K_{D,Fura}$ was assumed to be 276 nM as determined in the in vitro calibration. For EGTA we used $k_{on,EGTA} = 50$ μM^{-1} s^{-1} and $k_{off,EGTA} = 2.5$ s^{-1}, i.e., values close to the ones determined in Fig. 3. Fig. 4 *B* shows the calculated linear Ca^{2+} signals $[Ca^{2+}_L]$ (no correction for dye kinetics) and Fig. 4 *C* the corresponding corrected free Ca^{2+} transients (*thick lines*, (*1*)). The thin lines (*2*) in Fig. 4, *B* and *C*, show the best-fit integral components F_s and f_s, respectively (see Fig. 3 and Song et al., 1998).

Fig. 4 *D* shows the $k_{off,EGTA}$ values determined according to Song et al. (1998) for all simulated records when setting $K_{D,EGTA}$ in Eq. 3 to the true value used in the simulation. The α and $k_{off,EGTA}$ values (in s^{-1}) obtained in the fit were 2.87, 5.38, 13.6 and 2.66, 2.63, 2.69, respectively, for each of the three records shown in Fig. 4 *B*, and 2.73, 5.24, 13.4 and 2.53, 2.56, 2.67, respectively, for the free Ca^{2+} records shown in Fig. 4 *C*. The estimates of $k_{off,EGTA}$ are slightly above but very close to the true value (Fig. 4 *D*, *horizontal line*).

Fig. 4 *E* shows the result of determining both EGTA rate constants from the simulated data by using the $[Ca^{2+}]_0$ dependence of α. The continuous line in the figure was calculated using the true parameter values. Deviations from the line became noticeable only for $[Ca^{2+}]_0$ values larger than ~250 nM. In the range of $[Ca^{2+}]_0$ below 100 nM (*inset*) that was observed in the experiments of Fig. 3, the linear fit produced values very close to the ones used in the simulation: $k_{off,EGTA} = 2.65$ s^{-1} (vs. 2.5 s^{-1}) and $k_{on,EGTA} =$ 52.3 μM^{-1} s^{-1} (vs. 50 μM^{-1} s^{-1}). The parameter estimates were essentially independent of the correction for dye kinetics (*filled circles*: Ca^{2+}_L ; *open circles*: free Ca^{2+}). The values were $k_{off,EGTA} = 2.51$ s^{-1} and $k_{on,EGTA} = 52.3$ μM^{-1} s^{-1} when the free Ca^{2+} records were analyzed instead of $[Ca^{2+}_L](t)$.

In further simulations, troponin C as an additional intrinsic buffer was added to the reaction scheme, exhibiting fast Ca^{2+}-specific (T type) and slow parvalbumin-like (P type) binding sites of 240 μM each (rate constants according to Baylor and Hollingworth, 1998, values; see legend of Fig. 6 *B*). The estimated values of the rate constants were unchanged, showing that physiological intrinsic Ca^{2+} binding sites are unlikely to contribute significantly to the results under our conditions.

Determining indicator dye kinetics in the cell

Fura-2 Ca^{2+} measurements include low-pass-filtering due to the noninstantaneous binding of Ca^{2+} to the dye. The deconvolution to determine the true time course of rapid changes in free intracellular Ca^{2+} requires knowledge of the dissociation rate constant of the indicator (Klein et al., 1988). We applied an approach previously described for frog muscle fibers (Struk et al., 1998) to approximately determine the fura-2 dissociation rate constant $k_{off,Fura}$ in the cytoplasm of myotubes.

Under the conditions used here (high EGTA concentration), free $[Ca^{2+}]$ falls abruptly from the level reached at the end of the depolarization to a lower almost steady level (González and Ríos, 1993; Struk et al., 1998) due to the rapid termination of the Ca^{2+} flux. The almost stepwise change is demonstrated in the numerical simulation of Fig. 4 *C*. Here input flux is terminated instantaneously, and consequently

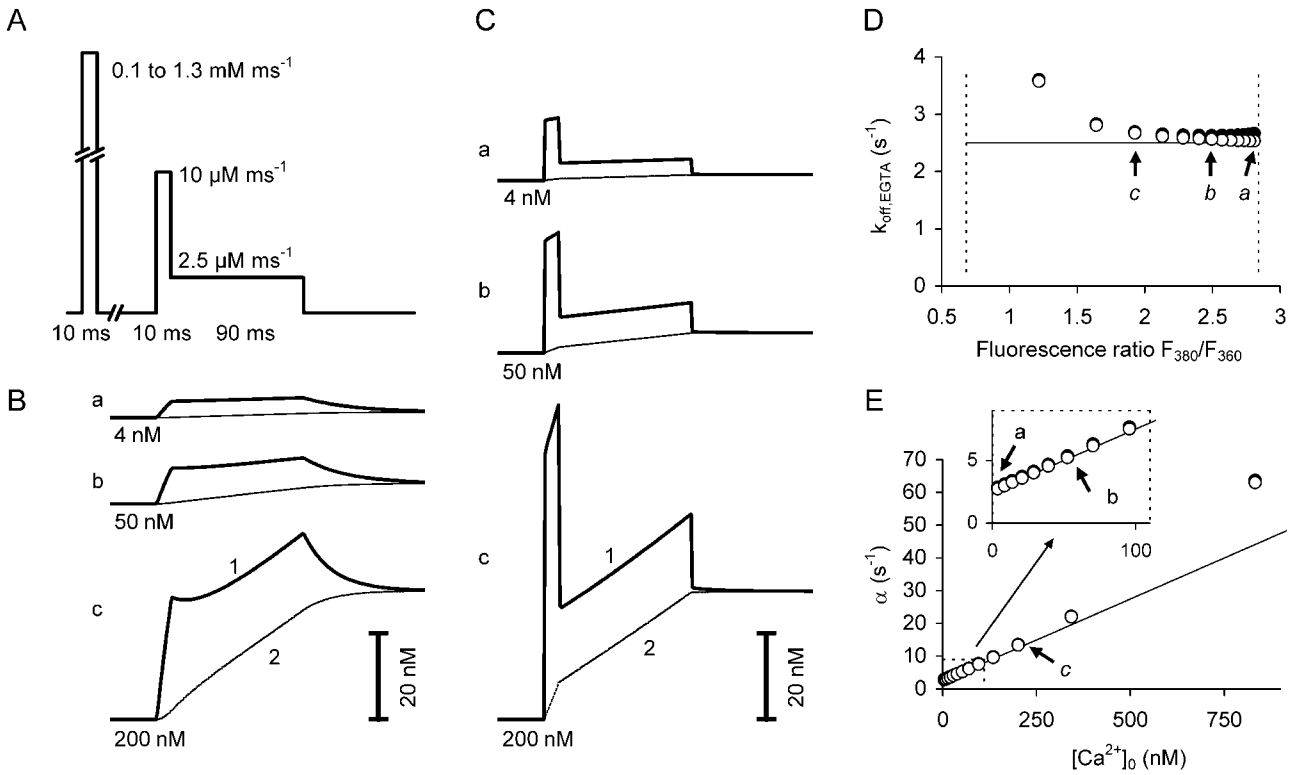

FIGURE 4 Simulation of Ca^{2+} transients to test the determination of buffer rate constants. (A) Artificial Ca^{2+} input flux records. The 10-ms prepulses create different levels of baseline Ca^{2+} concentration. The artificial flux signals were used as inputs to a system containing 200 μM fura-2 and 15 mM EGTA as described in the text. (*B*) Simulated "linear Ca^{2+}" records ($[Ca^{2+}_L]$, identical to free Ca^{2+} but low-pass-filtered by the dye kinetics). (*C*) Simulated free Ca^{2+} records. Numbers are baseline values. Thin lines (*2*) in *B* and *C* indicate the integral component F_s and f_s, respectively (see text for explanation). (*D*) $k_{off,EGTA}$ values determined from α according to Eq. 3. α was obtained by fitting the pedestal component of the simulated $[Ca^{2+}_L](t)$ traces (*filled circles*) as in Fig. 3 *C* or of the simulated free $[Ca^{2+}](t)$ traces (*open circles*). The horizontal line indicates the true $k_{off,EGTA}$ value used in the simulation. Dashed vertical lines indicate R_{max} and R_{min}. (*E*) Scaling factor α of the integral component (F_s, *filled circles*; f_s, *open circles*) as a function of the baseline Ca^{2+} concentration. In the low concentration range, a linear fit leads to the determination of $k_{on,EGTA}$ and $k_{off,EGTA}$ (*inset*); *a*, *b*, and *c* indicate the examples shown in *B* and *C*.

free Ca^{2+} shows a comparably rapid drop from the level reached at the end of the pulse to a new almost steady value (pedestal value). The fura-2 ratio signals (Fig. 5 *A*), on the other hand, decay with a single exponential time course that is determined by the fura-2 dissociation kinetics. The time constant τ of the exponential decay of dye-bound Ca^{2+}, given a stepwise change of free Ca^{2+}, depends on the free Ca^{2+} concentration (its level during the pedestal component) and the rate constants of the indicator (Eq. 5):

$$\tau = \frac{1}{k_{off,Fura} + k_{on,Fura} \cdot [Ca^{2+}]}. \quad (5)$$

Here $k_{off,Fura}$ and $k_{on,Fura}$ are dissociation and association rate constants of fura-2, respectively.

Eq. 5 can be rewritten in the form of Eq. 6:

$$\tau = \frac{1}{k_{off,Fura}} \cdot \frac{R - R_{max}}{R_{min} - R_{max}}. \quad (6)$$

Here, R is the fluorescence ratio value corresponding to the pedestal free Ca^{2+} level after repolarization. Single exponential fits to the fluorescence ratio records during the time interval after repolarization provide both a time constant τ and a final value R_∞. The fit is demonstrated in Fig. 5 *A* for the ratio signals corresponding to the three simulated free Ca^{2+} records of Fig. 4 *C*. The free Ca^{2+} value corresponding to R_∞ is a very good approximation of the almost constant free Ca^{2+} level after the end of repolarization (see Fig. 4 *C*). If R_{min} is known, $k_{off,Fura}$ and R_{max} can be determined by fitting a line to the plot of τ versus R_∞ as shown in Fig. 5 *B* for the complete set of ratio records generated in the simulation of Fig. 4. The examples shown in Fig. 5 *A* are indicated by the filled circles. The linear regression gave best-fit values of $k_{off,Fura}$ and R_{max} very close to the ones used in the simulations: 29.0 s^{-1} (vs. 30 s^{-1}) and 0.63 (vs. 0.68), respectively. When R_{min} and R_{max} were both set to their true values, $k_{off,Fura}$ was determined as 28.9 s^{-1}.

Fig. 5 *C* shows that the decay of the ratio signal in our experiments could in fact be fitted by a single exponential (plus a very slowly sloping line). Fig. 5 *D* summarizes the result from a series of background- and bleaching-corrected records of 11 cells (indicated by different symbols) that

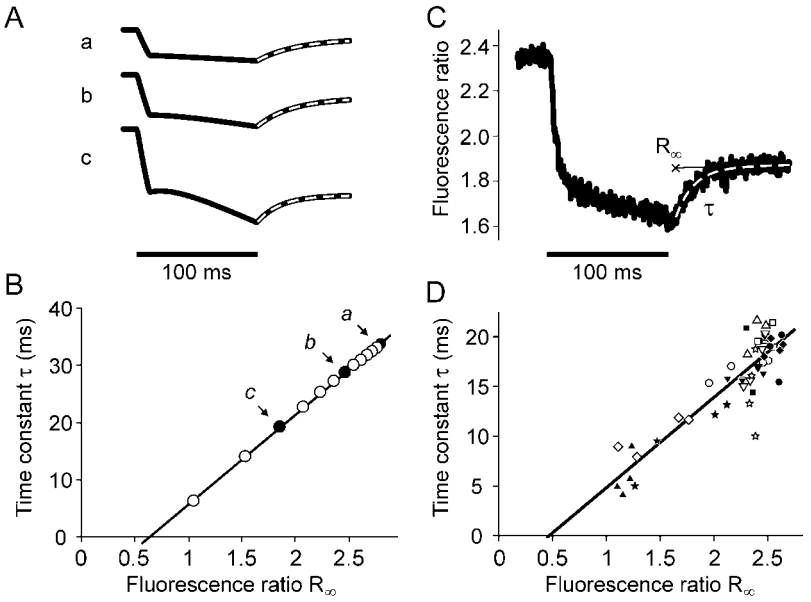

FIGURE 5 Experimental determination of indicator parameters. (*A*) Fluorescence ratio records generated by numerical simulation (same set of calculations as in Fig. 4, *B* and *C*). Single exponential fits to the decay time course are superimposed as dashed white lines on the relaxation phases. (*B*) Time constants of the single exponential component plotted versus final ratio level for all simulated records of Fig. 4 showing linear dependence according to Eq. 6 (*filled symbols* indicate the three records in *A*). (*C*) Measured fluorescence ratio signal and single exponential fit as in *A*. (*D*) Time constants obtained from different experimental records as the one in *C* plotted versus final ratio value (as in *B*). The continuous line shows the linear regression according to Eq. 6 with $k_{off,Fura}$ and R_{max} as free parameters.

covered a sufficient range of basal free Ca^{2+} (usually caused by appropriate prepulses). As in Fig. 5 *B*, the constant τ of the exponential component is plotted as a function of the end level R_∞ (after correction for the slow decay). The dependence could be fitted by a straight line according to Eq. 6. Values of the off-rate constant of fura-2 ($k_{off,Fura}$) and the steady-state calibration parameter R_{max} were returned by the least squares fit. R_{min} was set to 2.84 (see Methods). The best-fit parameter values obtained in this analysis were 46.4 $\pm$ 1.2 s^{-1} for $k_{off,Fura}$ and 0.47 $\pm$ 0.13 for R_{max} ($n = 44$). We consider the estimate for R_{max} obtained in this fit less reliable than the in vivo determination of R_{max} because of its large standard error and did not further use it for calculations. When setting both R_{min} and R_{max} to the values obtained in the in vivo calibration (2.84 and 0.68, respectively), a value for $k_{off,Fura}$ of 45.2 $\pm$ 0.9 s^{-1} was obtained that differed only slightly from the previous estimate. We used this value to calculate the time course of free myoplasmic Ca^{2+} from the fluorescence ratio signals according to Eq. 1 (see Methods).

Determination of free Ca^{2+} and Ca^{2+} input flux

Fig. 6 *A* demonstrates the kinetic deconvolution (using Eq. 1) for the record shown in Fig. 3 *B*. The calculation generates an initial peak in free myoplasmic Ca^{2+} that was not present in the indicator signal because the kinetics of Ca^{2+} binding to fura-2 is too slow. Its presence is only evident from the steeper slope at the beginning of the fluorescence trace. The free Ca^{2+} records obtained after the deconvolution were subjected to the same analysis as shown in Fig. 3. The integral component, here labeled f_s according to Song et al. (1998), and the result of subtracting it from the free Ca^{2+} trace (f_r, *thin line*) are shown in Fig. 6 *A*.

As in Fig. 3, a scaling factor α resulted from fitting the integral component f_s to the pedestal of f. Fig. 6 *C* plots α as a function of the baseline Ca^{2+} concentration for the same set of records as shown in Fig. 3 *D* but now after correction for dye kinetics. The linear fit to the data resulted in values of 2.12 $\pm$ 0.28 s^{-1} and 55.8 $\pm$ 7.3 μM^{-1} s^{-1} for $k_{off,EGTA}$ and $k_{on,EGTA}$, respectively. These values were finally used to determine the time course of EGTA-bound Ca^{2+} for the depolarization-induced Ca^{2+} recordings.

To determine the time course of the concentration of the total Ca^{2+} supplied to the myoplasmic space during the depolarization, bound and free Ca^{2+} concentration were summed. The input Ca^{2+} flux was calculated by taking the time derivative of the total Ca^{2+} change (Fig. 6 *B*). To obtain information on the possible contribution of intrinsic Ca^{2+} binding, we included in addition to fura-2 and EGTA also T and P sites originating from troponin C assuming concentration and properties as reported in the literature for mature muscle fibers (see Fig. 6 legend). The calculation showed that the troponin C components are negligibly small in comparison to the Ca^{2+} bound to EGTA. Correspondingly the resulting input Ca^{2+} fluxes with and without troponin C were essentially indistinguishable.

The phasic-tonic time course of the input flux seen in Fig. 6 *B* was found in most recordings, but Ca^{2+} transients and calculated input flux traces obtained in different myotubes showed considerable individual variability. We therefore averaged results of individual measurements that were obtained in different cells (Fig. 7). Panel *b* in Fig. 7 *A* (*thick line*) shows the mean fractional indicator occupancy derived from fluorescence ratio signals of 16 C2C12 cells when applying a voltage pulse of 100-ms duration to +20 mV (*a*). The thin lines in this and other panels indicate the standard errors of the mean. Panel *c* shows the mean of the individually determined input flux signals for the same group

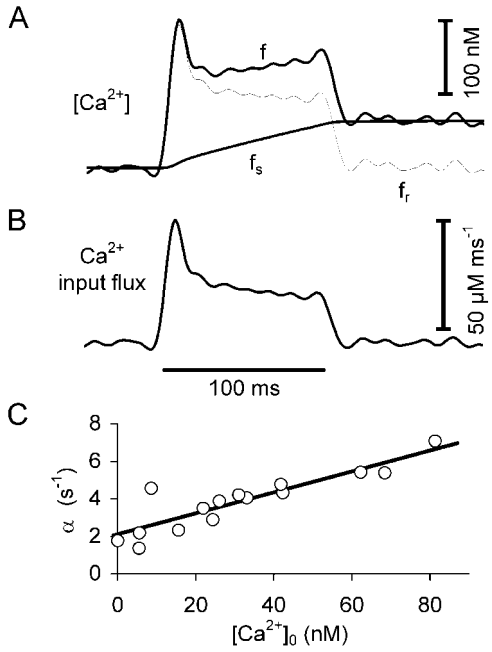

FIGURE 6 Calculation of free $[Ca^{2+}]$ and Ca^{2+} input flux and the use of free $[Ca^{2+}]$ records to determine $k_{on,EGTA}$ and $k_{off,EGTA}$. (*A*) Free Ca^{2+} concentration (*trace f*) derived from Fig. 3 *B* by solving Eq. 1. The trace f_s shows the integral component fitted to the pedestal. The thin line results from the subtraction of f_s. (*B*) Ca^{2+} input flux derived by taking the time derivative of total (free and bound) Ca^{2+}. Binding to intracellular sites (fura-2, EGTA, and troponin C) was calculated by using differential equations presented by Baylor et al. (1983) and Brum et al. (1988). The following set of model parameter values was used ($k_{on,X,Y}$, $k_{off,X,Y}$, and C_Y denote on- and off-rate constants for metal ion X (Ca^{2+} or Mg^{2+}) and binding component Y as well as concentration of Y): $R_{min} = \underline{2.84}$, $R_{max} = \underline{0.68}$, fura-2:$K_{D,Fura} = \underline{276\ nM}$, $k_{off,Ca,Fura} = \underline{45.2\ s^{-1}}$, $C_{Fura} = 200\ \mu M$. EGTA: $k_{on,Ca,EGTA} = \underline{55.8\ \mu M^{-1}\ s^{-1}}$, $k_{off,Ca,EGTA} = \underline{2.12\ s^{-1}}$. $C_{EGTA} = 15$ mM. T sites: $k_{on,Ca,T} = 88.5\ \mu M^{-1}\ s^{-1}$, $k_{off,Ca,T} = 115\ s^{-1}$, $C_T = 240\ \mu M$. P sites: $k_{on,Ca,P} = 41.7\ \mu M^{-1}\ s^{-1}$, $k_{off,Ca,P} = 0.5\ s^{-1}$, $k_{on,Mg,P} = 0.033\ \mu M^{-1}\ s^{-1}$, $k_{off,Mg,P} = 3\ s^{-1}$, $C_P = 240\ \mu M$, $C_{Mg,free} = 1$ mM). Omitting troponin C led to indistinguishable results. The underlined values were determined in the present study. (*C*) Scaling factor α of the integral component f_s obtained by fitting the pedestals (see *A*) as a function of baseline free $[Ca^{2+}]$. $k_{on,EGTA}$ and $k_{off,EGTA}$ are obtained as best-fit parameters from the linear regression (*continuous line*).

of measurements. On the other hand, panel *d* shows the input flux determined from the averaged ratio signal of panel *b*. Both approaches led to very similar results. Because calculating flux from the mean ratio signal is considerably less time-consuming than carrying out the individual calculations, it is convenient to use this calculation to obtain a rapid overview. Panel *e* of Fig. 7 *A* shows the corresponding averaged L-type current density and its standard error.

Comparison of C2C12 and primary myotubes

All measurements described so far were carried out in myotubes of the C2C12 cell line. Because many investigators use primary cultured myotubes, it was also of interest to see whether these two preparations differed in their calcium signaling characteristics. We therefore carried out the input flux determination as described above on fura-2 ratio signals of 16 primary-cultured mouse myotubes (Fig. 7 *B*). The conditions of the experiments were essentially identical.

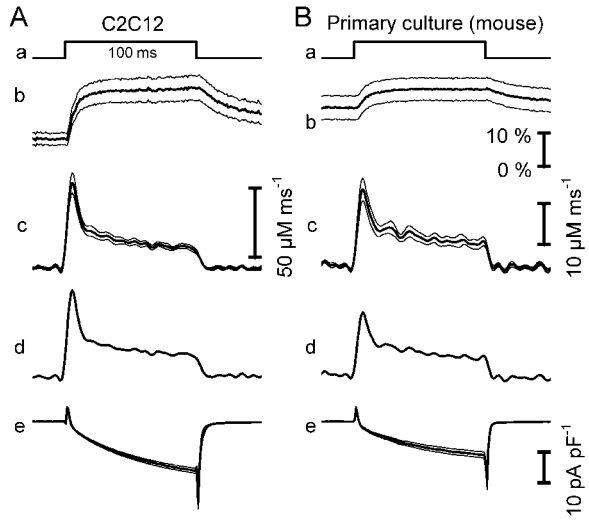

FIGURE 7 Comparison of C2C12 myotubes with primary cultured mouse myotubes. (*A*) C2C12 myotubes ($n = 16$). (*B*) Primary cultured mouse myotubes ($n = 16$). Traces show a comparison of fractional dye occupancy (*b*) Ca^{2+} input flux (*c* and *d*) and Ca^{2+} current density (*e*) induced by step depolarization to +20 mV (*a*). Records that showed no initial rapid phase in the ratio signal (as the one in Fig. 9 *E*) were excluded from this analysis. The averaged free Ca^{2+} concentrations (in nM) in the baseline from 100 to 10 ms before the pulse and at the end of the pulse (last 10 ms) were 28.6 ± 6.2 and 104.8 ± 22.8, respectively, for C2C12 and 72.7 ± 17.1 and 98.3 ± 18.8, respectively, for primary cultures. Both baseline free Ca^{2+} and peak Ca^{2+} input flux (62.1 ± 7.4 μM ms^{-1} in C2C12 and 19.2 ± 2.7 μM ms^{-1} in primary cultures) were significantly different according to student's double-sided *t*-test ($P < 0.05$). The results shown in *B* were obtained on a different setup. Therefore, $R_{min} = 3.5$, $R_{max} = 0.5$. Thin traces indicate mean ± SE.

In the analysis of the fluorescence signals, we applied the same set of parameters as determined for C2C12 myotubes. Only R_{min} and R_{max} were different, because the two groups of measurements were done on different setups. The baseline Ca^{2+} levels were significantly higher and the peak amplitudes of the Ca^{2+} input flux were significantly smaller in the primary cultured myotubes (see Fig. 7 legend). We cannot rule out a functional connection between these two differences. For instance, the elevated Ca^{2+} level may have caused a partial inactivation of Ca^{2+} release. The differences could, however, also be related to the fact that the C2C12 group contained larger cells (mean capacitance was 317 ± 22 pF in C2C12 compared to 107 ± 22 pF in primary myotubes). On the other hand, the general time course of both Ca^{2+} inward currents and input flux signals were not different in the two preparations.

Contribution of the Ca^{2+} inward current

The signals shown in Fig. 7 (*panels c* and *d*) are estimates of the total rate of Ca^{2+} entry into the myoplasm from both extracellular and intracellular sources. The component of the total Ca^{2+} input flux that enters the cell from the outside (Ca^{2+} entry flux) is proportional to the Ca^{2+} inward current density i_{Ca} (referred to linear membrane capacitance) and can therefore be calculated using Eq. 7 (assuming that the current is only carried by Ca^{2+} ions).

$$\frac{d[Ca^{2+}]}{dt}(i_{Ca}) = \frac{i_{Ca}}{z \cdot F \cdot f_V \cdot V_C}. \quad (7)$$

Here, z is the valence of the calcium ion (2), F the Faraday constant, V_C the intracellular volume per membrane capacitance, and f_V the fraction of the total volume that is immediately accessible to Ca^{2+}.

To assess V_C, we measured the cell volume with a confocal laser scanning microscope (see Methods) and simultaneously determined the capacitance by whole-cell recording. Capacitance proved to be proportional to volume (Fig. 8 *B*) as previously shown by Satoh et al. (1996) for cardiac myocytes. With the value of $V_C = 0.23\ l\ F^{-1}$ determined by linear regression and setting f_V to 1, we calculated the flux shown in Fig. 8 *D* using the mean Ca^{2+} current record of Fig. 7 *A* (*panel e*). Fig. 8 *C* shows for comparison the mean Ca^{2+} input flux of Fig. 7 *A* (*panel c*) displayed at a 10 times smaller scale than the trace in panel *D*. Comparing panel *C* and *D*, the mean amplitude ratio (average of values between 25 and 75 ms after onset of the pulse) was 79.3 ± 11.9 (n = 16). The result indicates that Ca^{2+} inward current makes only a small contribution to the Ca^{2+} input flux. Therefore, it can be concluded that under these experimental conditions the input flux consists mainly of Ca^{2+} release from the sarcoplasmic reticulum (SR). In some experiments (six in a total of 26 that were analyzed in this investigation), the recorded Ca^{2+} transients and consequently the calculated Ca^{2+} input fluxes were considerably smaller than in the cases discussed so far. Fig. 8 *E* shows one example. Not only is the flux amplitude considerably smaller than the one of the record in Fig. 8 *C*, also its time course is strikingly different. It rises slowly and shows a sharp peak at the end of the pulse and resembles the flux derived from the simultaneously measured Ca^{2+} inward current (Fig. 8 *F*). Apparently, in these cases internal Ca^{2+} release is essentially absent and the dye senses only the Ca^{2+} entering the myoplasm from the extracellular space.

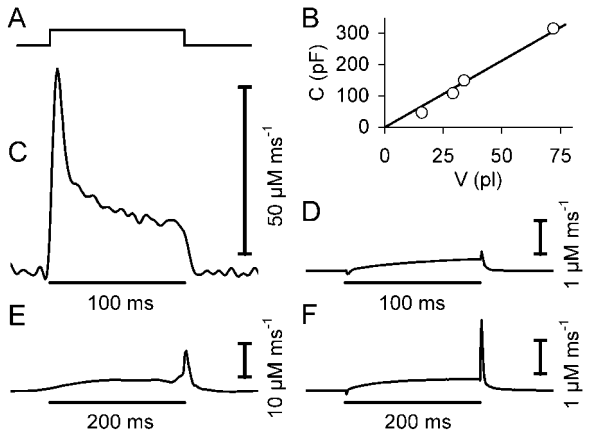

FIGURE 8 Comparison of total Ca^{2+} input flux and Ca^{2+} entry flux. (*A*) Scheme of the step depolarization. (*B*) Myotube volume versus membrane capacitance (*continuous line* shows a linear regression forced through the origin). (*C*) Mean Ca^{2+} input flux (same trace as in Fig. 7 *A*, *panel c*). (*D*) Ca^{2+} entry flux calculated using Eq. 7 from the mean Ca^{2+} current density of Fig. 7 *A* (*panel e*). The estimate of cell volume per capacitance (V_C) used in the calculation was obtained from the linear fit in *B*. The value was $V_C = 0.23 \pm 0.01\ l\ F^{-1}$. Note that *C* and *D* differ in scale by a factor of 10. (*E*) Ca^{2+} input flux in a myotube that probably showed no intracellular release. (*F*) Ca^{2+} entry flux calculated from the Ca^{2+} current measured during the same 200-ms depolarization to +40 mV that produced the signal in *E*. See text for further details.

Usually we focused on measurements with large Ca^{2+} transients and discontinued experiments that showed very small fluorescence transients. However, in cells without internal release, the measured Ca^{2+} inward current can serve as a control to check the fidelity of the Ca^{2+} flux calculation. Fig. 9 investigates the question of how well the flux generated by the Ca^{2+} inward current can be determined from fluorescence measurements. The calcium inward current shown in Fig. 9 *A* was first converted to flux by Eq. 7 and then scaled to reach the same amplitude during the pulse as the flux (*panel F*) derived from the simultaneously measured fluorescence signal (*panel E*). It was then used as input to a model containing EGTA and fura-2 as described in conjunction with Fig. 4 (parameters of Fig. 6 *B*). This generated the artificial fluorescence ratio record of panel *C*. Subsequently noise taken from a fluorescence recording at a subthreshold depolarization of the same experiment was added and the analysis procedure was applied to the noisy record (*panel D*) to derive the underlying input flux. The result is shown in panel *G*. Fig. 9 *H* shows the average of five records like the one in panel *G*, which were generated in the same way but using different experimental noise traces. Traces *G* and *H* are very similar to trace *F*, showing that the differences in time course between the flux calculated from the current and the one determined from the fluorescence signal result exclusively from the digital filtering necessary to cope with the higher noise level of the optical recording. Fig. 9 demonstrates that the shape of the optically recorded Ca^{2+} signal is in fact fully compatible with an underlying input flux that has the time course of the measured inward current.

DISCUSSION

Ca^{2+} signals in EGTA-buffered myoplasm

To interpret Ca^{2+} signals in terms of alterations in Ca^{2+}

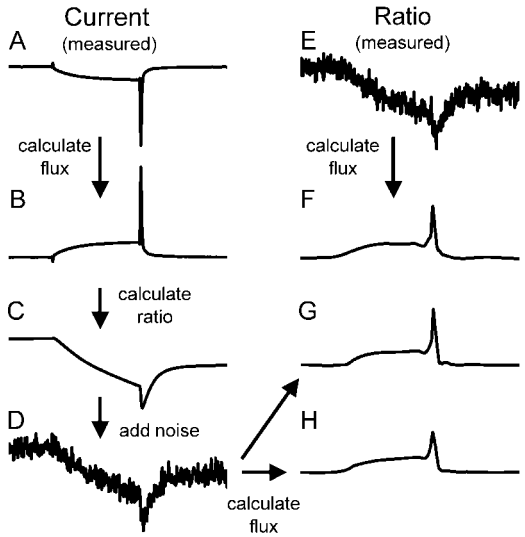

FIGURE 9 Ca^{2+} inward current-related flux. (*A*) Measured Ca^{2+} inward current density. (*B*) Ca^{2+} entry flux derived from *B* using Eq. 7. (*C*) Fluorescence ratio simulation using *B* as input and the set of parameter values of Fig. 6 *B*, however without troponin C. Signal scaled so that the amplitude during the depolarizing pulse matches the corresponding part of trace *F*. (*D*) Record *C* with noise added from a subthreshold fluorescence ratio record of the same experiment. (*E*) Fluorescence ratio record measured simultaneously with *A*. (*F*) Ca^{2+} input flux calculated from *E*. (*G*) Ca^{2+} input flux calculated from *D*. (*H*) Ca^{2+} input flux derived from average of five records as in *D* containing different experimental noise.

channel gating, the underlying flux of Ca^{2+} mobilization (Ca^{2+} input flux) has to be determined. In mature muscle fibers, both global and focal Ca^{2+} signals have been investigated in recent years to determine the overall Ca^{2+} input flux and the flux from a small group of SR Ca^{2+} release channels, respectively (for a recent review, see Ríos and Brum, 2002). Both approaches provided valuable complementary information on the function of the Ca^{2+} mobilization mechanism in skeletal muscle. Because protein expression in cultured myotubes has become a central tool for structure-function analysis in EC coupling (Beam and Franzini-Armstrong, 1997), it is important to pursue similar investigations in these cells. In the present study we analyzed global Ca^{2+} signals in voltage-clamped mouse muscle-derived myotubes with the goal to quantify the underlying Ca^{2+} input flux.

First attempts to derive the Ca^{2+} input flux in myotubes have been made in our laboratory (Dietze et al., 1998; Dietze et al., 2000; Ursu et al., 2001) by using the approach of Baylor et al. (1983). This method requires assumptions for the rate constants of intracellular Ca^{2+} binding sites to quantify the bound fraction of the mobilized Ca^{2+}. The present approach differs from the previous one by the direct experimental determination of kinetic parameters for the dominating intracellular Ca^{2+} buffer EGTA and the indicator dye fura-2 that were introduced into the cells. The procedure is derived from a method described by Song et al. (1998), who used millimolar concentrations of intracellular EGTA and a low affinity fast indicator dye to determine ''Ca^{2+} spikes'' in isolated heart cells. Because fura-2 does not bind calcium instantaneously, our experiments required a numerical deconvolution to determine the kinetics of free Ca^{2+}. On the other hand, the higher affinity of the indicator facilitated the measurement of the small Ca^{2+} transients in the strongly EGTA-buffered myoplasm and served to better resolve the pedestal Ca^{2+} components (at the end of the pulses) that were investigated in the analysis. Because fura-2 permitted ratiometric measurements, changes in basal free Ca^{2+} concentration could be separated from alterations in background fluorescence or indicator concentration changes. The ratiometric Ca^{2+} determination allowed us to estimate both rate constants of EGTA.

Determination of EGTA rate constants in the cell

The Ca^{2+} input flux calculation requires the quantification of all relevant Ca^{2+} binding compartments in the cell. At the very high concentration of EGTA in the pipette solution, it is unlikely that components other than EGTA make a significant additional contribution to intracellular Ca^{2+} binding (see also Pape et al., 1995; Song et al., 1998). Therefore, the rate constants and the concentration of EGTA in the cell are the essential determinants for the estimation of the Ca^{2+} input flux. If other slowly Ca^{2+} binding mechanisms made a significant contribution, they would be lumped together with EGTA in the analysis.

As pointed out by Song et al. (1998), the rate constant determination in their procedure becomes independent of the EGTA concentration at sufficiently high concentrations. Our pipette concentration of EGTA was 15 mM (compared to 4 mM in the previous experiments on heart cells), thus the conditions for applying the approximate equations derived by Song and co-workers were even better fulfilled. Conducting the analysis on simulated Ca^{2+} transients in a system with predefined parameters showed that the rate constants could in fact be determined quite precisely as long as signals were small enough not to saturate the dye appreciably (Fig. 4). It should be noted that the analysis generates ''apparent'' EGTA rate constants, which depend on certain assumptions, in particular on the value assumed for the dissociation constant of the indicator. The $K_{D,Fura}$ in the myotubes may be higher than found in vitro due to the binding of the indicator to intracellular proteins (Konishi et al., 1988). To test the effect on the calculation results, we increased $K_{D,Fura}$ to 500 nM. This is the mean of values listed by Pape et al. (1993). Table 1 compares the results obtained with the two different assumptions. The estimated apparent $K_{D,EGTA}$ constant increased more than twofold (mainly due to a change in the on rate constant). The calculated input flux, on the other hand, was much less affected by the change. It increased by only 25% and did not alter its time course.

The estimated EGTA rate constants were higher than

reported for in vitro conditions. $k_{off,EGTA}$ values of 0.3 s^{-1} (25°C and pH 7.0) and 0.5 s^{-1} (22°C and pH 7.2), and $k_{on,EGTA}$ values of 1.5 μM^{-1} s^{-1} and 2.7 μM^{-1} s^{-1}, respectively, were determined based on stopped-flow and temperature-jump relaxation experiments (Smith et al., 1984; Naraghi, 1997). We have no satisfying explanation for the difference, but noticed that other researchers, who likewise worked with high concentrations of EGTA in mammalian muscle cells and fitted EGTA rate constants to their measured Ca^{2+} transients, came to similar results: Shirokova et al. (1996) and Song et al. (1998) report $k_{off,EGTA}$ values of 3.4 s^{-1} (and higher) and 3 s^{-1}, respectively.

An advantage of the use of EGTA is that it binds most of the total released Ca^{2+} without significantly disturbing the local Ca^{2+} feedback mechanisms (Pape et al., 1995; Jong et al., 1995). This is a consequence of its slow kinetics and contrasts to the effect of faster buffers like BAPTA, which was found to eliminate the initial Ca^{2+} release peak in frog muscle fibers (Csernoch et al., 1993). A progress would be the use of a high concentration of a Ca^{2+} indicator with the binding properties of EGTA. This would allow to determine the Ca^{2+} input flux directly. Using the indicator Quin2, this approach was tried but not further pursued (Dey et al., 1996).

Determination of the fura off-rate constant in the cell

The deconvolution of the fura-2 signal to derive free Ca^{2+} depends on the knowledge of the indicator off-rate constant under cytoplasmic conditions (Eq. 1), which differs from in vitro measurements. Previous determinations of fura-2 rate constants in muscle cells used a dual dye approach. Klein et al. (1988) and Baylor and Hollingworth (1988) fitted Ca^{2+} records that were measured with the fast metallochromic indicator antipyrylazo III to simultaneously measured fura-2 records. A drawback of this method is that the calibration parameters of the fast indicator in the cell are likewise different from those obtained in vitro. To determine $k_{off,Fura}$ in our experiments, we used an alternative procedure that does not require measurements with a second dye. We made use of the fact, supported by simulations (this study) and measurements in frog fibers (Struk et al., 1998), that free calcium in the presence of high EGTA concentrations shows a step-like change when the input flux is rapidly terminated by repolarization (Fig. 4 *C*). Under these conditions, the Ca^{2+} occupancy of the indicator decays exponentially to a new equilibrium and the off-rate constant can be determined from the Ca^{2+} dependence of the time constant. The resulting value of 45.2 s^{-1} in this study was intermediate between intracellular determinations in mature muscle fibers (García and Schneider, 1993: 26 s^{-1} at 14–17°C) and in vitro determinations using temperature-jump relaxation or stopped-flow methods: 97 s^{-1} (Kao and Tsien, 1988) and 84 s^{-1} (Jackson et al., 1987).

TABLE 1 Differences in estimated parameter values and flux calculation caused by assuming two different values for $K_{D,Fura}$ in the cell

$K_{D,Fura}$	(nM)	276	500
R_{min}		2.84	2.77
$k_{off,Fura}$	(s^{-1})	45.2	46.6
$k_{on,EGTA}$	(μM^{-1} s^{-1})	55.8	31.8
$k_{off,EGTA}$	(s^{-1})	2.12	2.63
Flux peak	(μM ms^{-1})	60.9	76.0
Flux end level	(μM ms^{-1})	15.4	19.2
Peak/end level		3.95	3.97

See text for details.

Components of Ca^{2+} input flux

Ca^{2+} input flux consists of two main components: intracellular Ca^{2+} release and entry from the extracellular space. Because the voltage-activated Ca^{2+} current is proportional to the Ca^{2+} entry flux and can be recorded with high time resolution, it provides an independent control for our quantification of the input flux of Ca^{2+}. The input flux analysis in the cells with the smallest fluorescence changes led to results that showed characteristics of the electrically recorded inward current. Release from the SR is probably not functional in these myotubes and the recorded Ca^{2+} signal results from Ca^{2+} entering the cell with the L-type current. The reason for lack of internal release in part of the cells is unclear. If the expression of the ryanodine receptors was greatly reduced, L-type currents would be likewise reduced in amplitude due to compromised retrograde coupling. This was not observed. Probably gating of the ryanodine receptors is altered or loading of the SR not functional. In this context it should be mentioned that cells with apparently large Ca^{2+} release showed a variable degree of rundown (usually confined to the Ca^{2+} signals).

The electrically determined entry flux and the calculated input flux derived from the fluorescence transient shown in Fig. 8 differed in absolute scale. On average, when comparing the slowly changing sections of the signals (interval between 25 and 75 ms after pulse-on), the calculated input flux was larger by a factor of 10.5 ± 1.7 ($n = 8$). In these calculations, it was assumed that the effective cytoplasmic EGTA concentration is identical to the pipette concentration and that the whole cell volume is rapidly accessible to Ca^{2+} entering from the extracellular space ($f_v = 1$ in Eq. 7). Both assumptions are certainly overestimates. The EGTA concentration is probably smaller in the cell than in the pipette, but, given the loading velocity of the myotubes shown in Fig. 1 and assuming that EGTA diffuses comparably rapidly as fura-2, we guess that it is normally at least half the pipette value. Assuming that only 50% of the total cell volume is accessible for Ca^{2+} from the extracellular space ($f_V = 0.5$ in Eq. 7 as assumed by Sipido and Wier, 1991, for cardiac myocytes) the scale difference

comes down to a factor of ~2.5, which brings the differently obtained estimates quite close together.

The time course of the current-derived flux and the optically measured flux in cells without intracellular release was similar but not identical. Fig. 9 demonstrates that, due to noise in the optical signals and the necessary digital filtering, the sharp peak in the flux arising from the tail current was underestimated by a factor of ~50% compared with the slowly changing signal components. However, these small signals with their low signal-to-noise ratio present particularly unfavorable conditions for the analysis. The signal-to-noise ratio is higher in the larger fluorescence signals. Thus, equally fast flux components underlying larger Ca^{2+} transients are likely to be less affected by the digital filtering and therefore better resolved.

The input flux derived from the larger fluorescence signals showed a completely different time course exhibiting a leading peak and a decline to a lower, slowly declining level. It originates mainly from intracellular Ca^{2+} release. C2C12 myotubes contain voltage- and ligand-activatable Ca^{2+} pools that form part of the same intracellular Ca^{2+} store (Lorenzon et al., 2000). This notion was based on experiments in which depolarizing solutions with elevated K^+ concentration were applied and combined with caffeine stimulation. K^+ responses could be suppressed by conditioning caffeine application and vice versa. The fact that depolarization elicited Ca^{2+} transients in the absence of extracellular Ca^{2+} shows that C2C12 myotubes develop skeletal muscle-type EC coupling. Whereas Györke and Györke (1996) reported that K^+, like caffeine, released Ca^{2+} at discrete loci, Lorenzon et al. (2000) described a rapid, spatially synchronous elevation of intracellular Ca^{2+} when the cells were superfused with Ca^{2+}-free depolarizing solutions. In voltage-clamped primary-cultured mouse myotubes, Shirokova et al. (1999) observed inhomogeneous Ca^{2+} release evidenced by narrow zones that were not responsive to depolarization. Even though the intracellular organization of the Ca^{2+} stores in myotubes is obviously more heterogeneous and less orderly than in mature muscle fibers, the previous and our present experimental evidence strongly suggests that C2C12 myotubes, like primary-cultured myotubes, share great similarities in EC coupling with mature fibers. Our experiments demonstrate that the characteristics of the depolarization-activated Ca^{2+} flux in C2C12 myotubes and mouse primary-cultured myotubes are very similar. The majority of measurements from both preparations showed phasic-tonic Ca^{2+} input flux signals that resemble the Ca^{2+} release rate records measured in mature mammalian skeletal muscle fibers under similar intracellular conditions (Shirokova et al., 1996). According to current models, the initial peak of the Ca^{2+} release flux has strong contributions from a Ca^{2+}-dependent positive feedback mechanism (calcium-induced calcium release) whereas the release activity that follows the peak is predominantly voltage-gated (Csernoch et al., 1993; Stern et al., 1997). Further studies are required to verify if these concepts can be also applied in unmodified form to EC coupling in myotubes.

In conclusion, the results indicate that the present procedure leads to a reliable reconstruction of the time course of global Ca^{2+} input flux in myotubes. As in primary cultured myotubes, the flux estimated in C2C12 myotubes shows great similarities to the voltage-activated Ca^{2+} release flux in muscle fibers. Normally, Ca^{2+} inward current makes only a small contribution to the total flux signal even at the high concentration of 10 mM Ca^{2+} used in our external solution. The effect of the inward current will, however, become discernible when depletion of the SR takes place or when the Ca^{2+} tail current measured on repolarization is large or slowed down. The high-EGTA method is a straightforward way to gain insight into the dynamics of cellular Ca^{2+} fluxes and should therefore be of value for structure-function analyses in myotube preparations used for expression of EC coupling proteins.

We are grateful to Dr. H. Brinkmeier for advice regarding the cell culture, to E. Schoch for designing and constructing valuable setup devices, and to Dr. K. Föhr for providing software for the calculation of binding equilibria. We also thank W. Fritz and E. Schmid for help with the carbon-coating of coverslips and U. Pika-Hartlaub, M. Rudolph-Dauner, S. Schäfer, and U. Richter for excellent technical help with cell culture and solutions.

The work was supported by a grant of the Deutsche Forschungsgemeinschaft to W. Melzer (ME-713/10-2) and a scholarship of the Graduiertenkolleg 182 to R.P. Schuhmeier.

REFERENCES

Baylor, S. M., W. K. Chandler, and M. W. Marshall. 1983. Sarcoplasmic reticulum calcium release in frog skeletal muscle fibres estimated from Arsenazo III calcium transients. *J. Physiol.* 344:625–666.

Baylor, S. M., and S. Hollingworth. 1988. Fura-2 calcium transients in frog skeletal muscle fibres. *J. Physiol.* 403:151–192.

Baylor, S. M., and S. Hollingworth. 1998. Model of sarcomeric Ca^{2+} movements, including ATP Ca^{2+} binding and diffusion, during activation of frog skeletal muscle. *J. Gen. Physiol.* 112:297–316.

Baylor, S. M., and S. Hollingworth. 2000. Measurement and interpretation of cytoplasmic [Ca^{2+}] signals from calcium indicator dyes. *News Physiol. Sci.* 15:19–26.

Beam, K. G., and C. Franzini-Armstrong. 1997. Functional and structural approaches to the study of excitation-contraction coupling. *Methods Cell Biol.* 52:283–306.

Bers, D. M. 2001. Excitation-Contraction Coupling and Cardiac Contractile Force. Kluwer Academic Publishers, Dordrecht, The Netherlands.

Blau, H. M., C. P. Chiu, and C. Webster. 1983. Cytoplasmic activation of human nuclear genes in stable heterocaryons. *Cell.* 32:1171–1180.

Brum, G., E. Ríos, and E. Stefani. 1988. Effects of extracellular calcium on calcium movements of excitation-contraction coupling in frog skeletal muscle fibres. *J. Physiol.* 398:441–473.

Brum, G., E. Stefani, and E. Ríos. 1987. Simultaneous measurements of Ca^{2+} currents and intracellular Ca^{2+} concentrations in single skeletal muscle fibers of the frog. *Can. J. Physiol. Pharmacol.* 65:681–685.

Chaudhari, N. 1992. A single nucleotide deletion in the skeletal muscle-specific calcium channel transcript of muscular dysgenesis (mdg) mice. *J. Biol. Chem.* 267:25636–25639.

Csernoch, L., V. Jacquemond, and M. F. Schneider. 1993. Microinjection of strong calcium buffers suppresses the peak of calcium release during

depolarization in frog skeletal muscle fibers. *J. Gen. Physiol.* 101:297–333.

Dey, S. K., M. G. Klein, and M. F. Schneider. 1996. SR calcium release determination in quin-2 buffered frog cut skeletal muscle fibers. *Biophys. J.* 70:A167.

Dietze, B., F. Bertocchini, V. Barone, A. Struk, V. Sorrentino, and W. Melzer. 1998. Voltage-controlled Ca^{2+} release in normal and ryanodine receptor type 3 (RyR3)-deficient mouse myotubes. *J. Physiol.* 513:3–9.

Dietze, B., J. Henke, H. M. Eichinger, F. Lehmann-Horn, and W. Melzer. 2000. Malignant hyperthermia mutation Arg615Cys in the porcine ryanodine receptor alters voltage dependence of Ca^{2+} release. *J. Physiol.* 526:507–514.

Dirksen, R. T. 2002. Bi-directional coupling between dihydropyridine receptors and ryanodine receptors. *Front. Biosci.* 7:d659–670.

Fessenden, J. D., Y. Wang, R. A. Moore, S. R. Chen, P. D. Allen, and I. N. Pessah. 2000. Divergent functional properties of ryanodine receptor types 1 and 3 expressed in a myogenic cell line. *Biophys. J.* 79:2509–2525.

Flucher, B. E., N. Kasielke, and M. Grabner. 2000. The triad targeting signal of the skeletal muscle calcium channel is localized in the COOH terminus of the alpha(1S) subunit. *J. Cell Biol.* 151:467–478.

Föhr, K. J., W. Warchol, and M. Gratzl. 1993. Calculation and control of free divalent cations in solutions used for membrane fusion studies. *Methods Enzymol.* 221:149–157.

Friedrich, O., T. Ehmer, and R. H. Fink. 1999. Calcium currents during contraction and shortening in enzymatically isolated murine skeletal muscle fibres. *J. Physiol.* 517:757–770.

García, J., and M. F. Schneider. 1993. Calcium transients and calcium release in rat fast-twitch skeletal muscle fibres. *J. Physiol.* 463:709–728.

García, J., T. Tanabe, and K. G. Beam. 1994. Relationship of calcium transients to calcium currents and charge movements in myotubes expressing skeletal and cardiac dihydropyridine receptors. *J. Gen. Physiol.* 103:125–147.

Gasser, T., H. G. Müller, and A. R. Marks. 1985. Kernels for nonparametric curve estimation. *J. Roy. Stat. Soc. B.* 47:238–252.

González, A., and E. Ríos. 1993. Perchlorate enhances transmission in skeletal muscle excitation-contraction coupling. *J. Gen. Physiol.* 102:373–421.

Grabner, M., R. T. Dirksen, N. Suda, and K. G. Beam. 1999. The II–III loop of the skeletal muscle dihydropyridine receptor is responsible for the bi-directional coupling with the ryanodine receptor. *J. Biol. Chem.* 274:21913–21919.

Györke, I., and S. Györke. 1996. Adaptive control of intracellular Ca^{2+} release in C2C12 mouse myotubes. *Pflugers Arch.* 431:838–843.

Jackson, A. P., M. P. Timmerman, C. R. Bagshaw, and C. C. Ashley. 1987. The kinetics of calcium binding to fura-2 and indo-1. *FEBS Lett.* 216:35–39.

Jong, D. S., P. C. Pape, S. M. Baylor, and W. K. Chandler. 1995. Calcium inactivation of calcium release in frog cut muscle fibers that contain millimolar EGTA or Fura-2. *J. Gen. Physiol.* 106:337–388.

Jurkat-Rott, K., U. Uetz, U. Pika-Hartlaub, J. Powell, B. Fontaine, W. Melzer, and F. Lehmann-Horn. 1998. Calcium currents and transients of native and heterologously expressed mutant skeletal muscle DHP receptor alpha1 subunits (R528H). *FEBS Lett.* 423:198–204.

Kao, J. P., and R. Y. Tsien. 1988. Ca^{2+} binding kinetics of fura-2 and azo-1 from temperature-jump relaxation measurements. *Biophys. J.* 53:635–639.

Klein, M. G., B. J. Simon, G. Szücs, and M. F. Schneider. 1988. Simultaneous recording of calcium transients in skeletal muscle using high- and low-affinity calcium indicators. *Biophys. J.* 53:971–988.

Konishi, M., A. Olson, S. Hollingworth, and S. M. Baylor. 1988. Myoplasmic binding of fura-2 investigated by steady-state fluorescence and absorbance measurements. *Biophys. J.* 54:1089–1104.

Lorenzon, P., F. Grohovaz, and F. Ruzzier. 2000. Voltage- and ligand-gated ryanodine receptors are functionally separated in developing C2C12 mouse myotubes. *J. Physiol.* 525:499–507.

Melzer, W., A. Herrmann-Frank, and H. C. Lüttgau. 1995. The role of Ca^{2+} ions in excitation-contraction coupling of skeletal muscle fibres. *Biochim. Biophys. Acta.* 1241:59–116.

Moore, R. A., H. Nguyen, J. Galceran, I. N. Pessah, and P. D. Allen. 1998. A transgenic myogenic cell line lacking ryanodine receptor protein for homologous expression studies: reconstitution of RyR1 protein and function. *J. Cell Biol.* 140:843–851.

Müller, H. G., and U. Stadtmüller. 1987. Variable bandwidth kernel estimators of regression curves. *Ann. Stat.* 15:182–201.

Naraghi, M. 1997. T-jump study of calcium binding kinetics of calcium chelators. *Cell Calcium.* 22:255–268.

Pape, P. C., D. S. Jong, and W. K. Chandler. 1995. Calcium release and its voltage dependence in frog cut muscle fibers equilibrated with 20 mM EGTA. *J. Gen. Physiol.* 106:259–336.

Pape, P. C., D. S. Jong, W. K. Chandler, and S. M. Baylor. 1993. Effect of fura-2 on action potential-stimulated calcium release in cut twitch fibers from frog muscle. *J. Gen. Physiol.* 102:295–332.

Powell, J. A., L. Petherbridge, and B. E. Flucher. 1996. Formation of triads without the dihydropyridine receptor alpha subunits in cell lines from dysgenic skeletal muscle. *J. Cell Biol.* 134:375–387.

Ratzlaff, K. L. 1987. Polynomial least squares convolution techniques. *In* Introduction to Computer-Assisted Experimentation. Wiley, New York. 384–396.

Rice, J. 1984. Bandwidth choice for nonparametric regression. *Ann. Stat.* 12:1215–1230.

Ríos, E., and G. Brum. 2002. Ca^{2+} release flux underlying Ca^{2+} transients and Ca^{2+} sparks in skeletal muscle. *Front. Biosci.* 7:d1195–d1211.

Ríos, E., and G. Pizarro. 1991. Voltage sensor of excitation-contraction coupling in skeletal muscle. *Physiol. Rev.* 71:849–908.

Satoh, H., L. M. Delbridge, L. A. Blatter, and D. M. Bers. 1996. Surface:volume relationship in cardiac myocytes studied with confocal microscopy and membrane capacitance measurements: species-dependence and developmental effects. *Biophys. J.* 70:1494–1504.

Savitzky, A., and M. J. E. Golay. 1964. Smoothing and differentiation of data by simplified least squares procedures. *Anal. Chem.* 36:1627–1639.

Schneider, M. F. 1994. Control of calcium release in functioning skeletal muscle fibers. *Annu. Rev. Physiol.* 56:463–484.

Shirokova, N., J. García, G. Pizarro, and E. Ríos. 1996. Ca^{2+} release from the sarcoplasmic reticulum compared in amphibian and mammalian skeletal muscle. *J. Gen. Physiol.* 107:1–18.

Shirokova, N., R. Shirokov, D. Rossi, A. González, W. G. Kirsch, J. García, V. Sorrentino, and E. Ríos. 1999. Spatially segregated control of Ca^{2+} release in developing skeletal muscle of mice. *J. Physiol.* 521:483–495.

Sipido, K. R., and W. G. Wier. 1991. Flux of Ca^{2+} across the sarcoplasmic reticulum of guinea-pig cardiac cells during excitation-contraction coupling. *J. Physiol.* 435:605–630.

Smith, P. D., G. W. Liesegang, R. L. Berger, G. Czerlinski, and R. J. Podolsky. 1984. A stopped-flow investigation of calcium ion binding by ethylene glycol bis(beta-aminoethyl ether)-N,N′-tetraacetic acid. *Anal. Biochem.* 143:188–195.

Song, L. S., J. S. Sham, M. D. Stern, E. G. Lakatta, and H. Cheng. 1998. Direct measurement of SR release flux by tracking 'Ca^{2+} spikes' in rat cardiac myocytes. *J. Physiol.* 512:677–691.

Stern, M. D., G. Pizarro, and E. Ríos. 1997. Local control model of excitation-contraction coupling in skeletal muscle. *J. Gen. Physiol.* 110:415–440.

Struk, A., G. Szücs, H. Kemmer, and W. Melzer. 1998. Fura-2 calcium signals in skeletal muscle fibres loaded with high concentrations of EGTA. *Cell Calcium.* 23:23–32.

Szentesi, P., C. Collet, S. Sarkozi, C. Szegedi, I. Jona, V. Jacquemond, L. Kovács, and L. Csernoch. 2001. Effects of dantrolene on steps of excitation-contraction coupling in mammalian skeletal muscle fibers. *J. Gen. Physiol.* 118:355–375.

Takekura, H., M. Nishi, T. Noda, H. Takeshima, and C. Franzini-Armstrong. 1995. Abnormal junctions between surface membrane and

sarcoplasmic reticulum in skeletal muscle with a mutation targeted to the ryanodine receptor. *Proc. Natl. Acad. Sci. USA*. 92:3381–3385.

Timmer, J., T. Müller, and W. Melzer. 1998. Numerical methods to determine calcium release flux from calcium transients in muscle cells. *Biophys. J*. 74:1694–1707.

Ursu, D., S. Sebille, B. Dietze, D. Freise, V. Flockerzi, and W. Melzer. 2001. Excitation-contraction coupling in skeletal muscle of a mouse lacking the dihydropyridine receptor subunit gamma1. *J. Physiol*. 533:367–377.

Wang, S. Q., L. S. Song, E. G. Lakatta, and H. Cheng. 2001. Ca^{2+} signalling between single L-type Ca^{2+} channels and ryanodine receptors in heart cells. *Nature*. 410:592–596.

Yaffe, D., and O. Saxel. 1977. Serial passaging and differentiation of myogenic cells isolated from dystrophic mouse muscle. *Nature*. 270:725–727.